



Ionic liquid treatment of flax fibers and the effects on morphology and mechanical properties

Lukas Pachernegg-Mair^{a,b,*}, Jana B. Schaubeder^a, August Brandberg^c, Michael Thoman^a, Georg Urstöger^d, Markus Rüggeberg^e, Kristie J. Koski^f, Harald Plank^{g,h}, Ulrich Hirn^a, Stefan Spirk^{a,b}, Caterina Czibula^{a,**}

^a Institute of Bioproducts and Paper Technology, Graz University of Technology, Inffeldgasse 23, 8010, Graz, Austria

^b Ecolyte GmbH, Puchstraße 17, 8020, Graz, Austria

^c Lightness By Design AB, Stockholm, SE-111 30, Sweden

^d Anton Paar GmbH, Anton-Paar-Straße 20, 8054, Graz, Austria

^e Institute for Forest Utilization and Forest Technology, Dresden University of Technology, Piennner Straße 19, 01737, Tharandt, Germany

^f Department of Chemistry, University of California Davis, 1 Shields Ave. 222 Chemistry, Davis, CA, 95616, United States of America

^g Institute of Electron Microscopy, Graz University of Technology, Steyrergasse 17, 8010, Graz, Austria

^h Graz Center of Electron Microscopy, Steyrergasse 17, 8010, Graz, Austria

ARTICLE INFO

Keywords:

Cellulosic fibers
Ionic liquid
Atomic force microscopy
Wide-angle x-ray scattering
Mechanical properties
Brillouin spectroscopy
Flax fiber

ABSTRACT

The structure of the cell walls of plant fibers, comprising cellulose microfibrils embedded in a matrix (hemicelluloses, lignin, and/or pectin) plays a crucial role for their mechanical behavior. However, the direct measurement of the cell wall structure remains challenging, and the effects of their partial dissolution on mechanical properties are poorly understood. Although, with growing environmental awareness more industrial applications and production routines based on dissolution of lignocellulosic materials are being explored. Here, we demonstrate the time-dependent dissolution of flax fibers using the ionic liquid 1-ethyl-3-methylimidazolium acrylate [EMIM][ACR] to better understand the influence of the fiber structure and its dissolution on the mechanical properties. The treatment progressively dissolves the outer layers (primary wall and S1 layer) of isolated single fibers, providing access to the S2 layer. Atomic force microscopy (AFM) revealed cellulose microfibril angles closely aligning with wide-angle X-ray scattering (WAXS) results (AFM: $5.7 \pm 1.9^\circ$; WAXS: $5.0 \pm 1.6^\circ$). Tensile testing showed significant reductions in mechanical properties with treatment duration, while Brillouin spectroscopy revealed small changes in axial stiffness (C_{33}), dominated by the microfibrils, but a substantial decrease in shear modulus $G = 12.0 \text{ GPa} - 4.6 \text{ GPa}$, highlighting matrix dissolution. Combining AFM, WAXS, tensile testing, and Brillouin spectroscopy provides a comprehensive understanding of the dissolution process and its effects on flax fiber structure and mechanics.

1. Introduction

Rising demand for sustainable and high-performance materials has brought plant fiber-based materials to the forefront of materials science. Natural fibers offer a combination of mechanical strength, lightweight characteristics, and environmental sustainability [1,2]. Possible applications range from stand-alone materials, e.g., cellulose-based foams [3, 4] to composite materials [1,2]. The use of these materials, however,

requires deep understanding of the structure-mechanical property relationships of lignocellulosic fibers. Usually, the industrial production of lignocellulosic fibers requires the use of harsh chemicals e.g., during kraft pulping [5], altering the structure and composition of the material. In scientific literature, the use of more selective processes e.g., organosolv pulping [6–8] or the use of ionic liquids (ILs) [9–11] has gained traction since it enables the better utilization of biomass [12]. Although, these processes use less harsh conditions, they still alter the

This article is part of a special issue entitled: Nanomechanical Testing 2024 published in Materials Science & Engineering A.

* Corresponding author. Institute of Bioproducts and Paper Technology, Graz University of Technology, Inffeldgasse 23, 8010, Graz, Austria.

** Corresponding author.

E-mail addresses: lpachernegg@tugraz.at (L. Pachernegg-Mair), caterina.czibula@tugraz.at (C. Czibula).

<https://doi.org/10.1016/j.msea.2025.148675>

Received 20 March 2025; Received in revised form 29 May 2025; Accepted 11 June 2025

Available online 12 June 2025

0921-5093/© 2025 The Author(s). Published by Elsevier B.V. This is an open access article under the CC BY license (<http://creativecommons.org/licenses/by/4.0/>).

structure-mechanical property relationships by disintegrating the natural fiber composite [12]. Especially the use of ILs enables a highly selective dissolution of the lignocellulosic material [13,14], enabling the optimization of the fiber material for its designated use.

One of the main limitation of using natural fibers as reinforcing material for composites are the moisture adsorption and lack of affinity between fiber and matrix. Here, various physical (e.g. steam explosion, plasma treatment), biochemical (e.g. enzymatic and fungi) or chemical (e.g. acetylation, alkali, or peroxide treatments) treatments of the fibers are explored, which alter the fiber's properties to different extends with the ultimate goal to improve the adhesion property between fiber and matrix [15–18].

Among these natural cellulose-based fiber materials, phloem flax fibers stand out with their high cellulose content (>70 %) and relatively low lignin content (<3 %). Additionally, pectin and a small amount of waxes (<2 %) are present in flax fibers, especially in the outer layers of the fiber [5,19–23]. Further flax fibers do not require the use of harsh chemicals during production [24], minimizing the impact on the structure-mechanical property relationship. This makes them an excellent model system for studying the influence of treatments [25,26].

The mechanical behavior of lignocellulosic fibers is governed by their hierarchical cell wall structure, which consists of primary (P) and

secondary (S) wall layers, see Fig. 1. Where the S2 layer plays a dominant role in mechanical strength and stiffness. Understanding the mechanical properties of the S2 layer is essential to better understand natural fiber materials. The primary cell wall contains typically cellulose microfibrils, aggregated into bundles, often termed microfibril bundles (macrofibrils) with random alignment. Next, the secondary cell wall can be separated into three distinct layers: S1, S2 and S3. The S2 layer is composed of highly orientated microfibrils, which, in many cases, are closely aligned to the axial fiber direction with the so-called microfibril angle (MFA) ranging typically between 5° and 20°, though it can vary by species, location, tissue type, and maturity of the plant. Both, in the S1 and S3 layer, the microfibrils may be oriented in helices of opposite sign (so-called S and Z helices), whereas especially in the S1 layer microfibrils are often oriented perpendicular to the fiber axis. The MFA values in the S3 layer exceed often 40° [27–34].

The MFA values of cellulosic fibers are commonly assessed by X-ray techniques such as small angle X-ray scattering (SAXS) or wide-angle X-ray scattering (WAXS), as well as by optical approaches such as confocal microscopy, polarization microscopy, second-harmonic generation imaging under controlled polarized light (P-SHG) and atomic force microscopy (AFM) [30,31,35,36]. However, these techniques often probe entire fibers or outer layer surfaces, rather than isolating specific sublayers, which is important if one tries to better understand the underlying influencing factors.

While ionic liquids (ILs) have been widely studied for lignocellulosic fiber dissolution [9–11], the precise mechanisms by which ILs interact with cellulose and other compounds at the molecular level—particularly in the context of fiber sublayers—are not yet fully understood [37–42]. However, there is agreement that the dissolution begins at the fiber's outer layers, where IL accessibility is highest, and progresses inward to the core, as shown in studies by Ghasemi et al. [39], Chen et al. [43] and Villar et al. [44].

In this study, we introduce a novel approach to selectively dissolve untreated flax fibers using IL-induced partial dissolution starting from the outer layers. By changing the ILs exposure time, we aim to access and characterize the S2 layer directly while simultaneously trying to understand the influence on mechanical properties.

Specifically, we employ 1-ethyl-3-methylimidazolium acrylate ([EMIM][ACR]), an IL chosen for its moderated dissolution kinetics compared to conventional ILs capable of dissolving cellulose. In comparison to the more common acetate anion, the acrylate anion introduces steric hindrance and reduced hydrogen bond strength, allowing for a controlled dissolution process that keeps the fiber's structure intact [45–47].

To quantitatively assess the impact of IL treatment, we combine AFM and WAXS to investigate microfibril alignment and diameter changes with tensile testing and Brillouin spectroscopy to probe mechanical properties [22,48,49]. The use of Brillouin spectroscopy, a non-contact optical technique, in addition to tensile testing, allows us to measure the elastic properties of IL-treated and untreated single fibers along the axial fiber direction. This provides us with vital information on the normal and shear stiffness. The principle of Brillouin light scattering is based on the inelastic interaction of laser light with acoustic phonons in a material [50,51]. Apart from its non-contact approach, the advantage of Brillouin spectroscopy is that it enables the measurement of all elastic stiffness tensor components, therefore, providing the complete mechanical properties also for anisotropic materials like fibers. Here, biological materials such as collagen [52], fibrous proteins [53], spider silk [54], bamboo fibers [55], and marine sponges [56] were studied in the literature. Previously, the anisotropy of plant fibers was analyzed [57], and we have investigated the elastic stiffness tensor of viscose fibers [58] and the transverse modulus of different wood-based cellulose fibers [59].

With this combined approach we want to answer how the IL-induced partial dissolution affects the structural integrity and mechanical properties of flax fibers. The approach offers new insights into the interplay

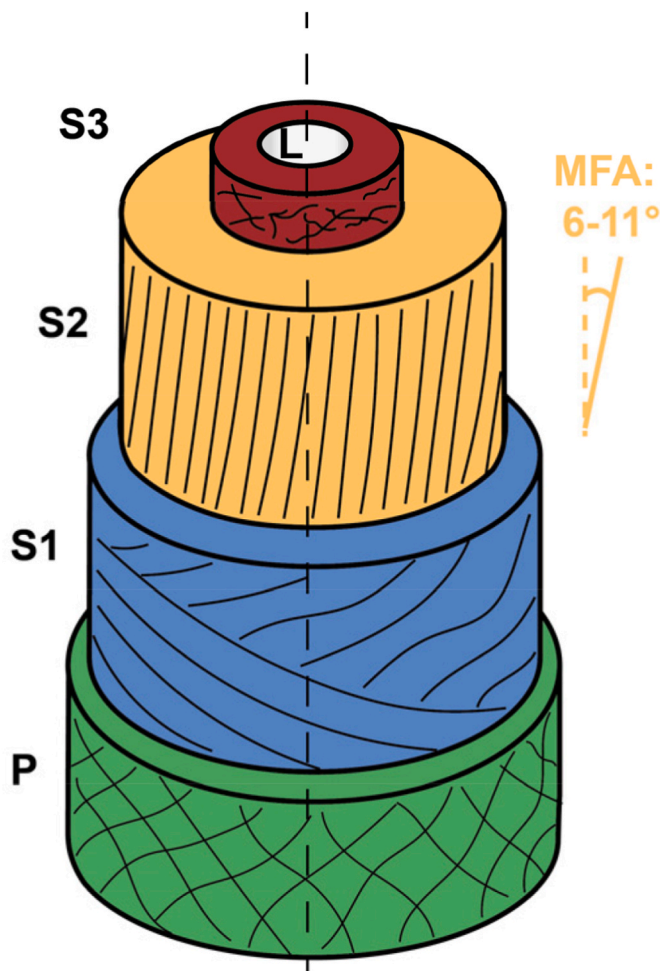


Fig. 1. Structure of a flax fiber cell wall illustrating the different cell wall layers and their corresponding microfibril orientation. The cell wall is made of the primary wall (P), the secondary wall (S1, S2, S3) and the lumen (L) at its center (Reprinted and adapted from *Composites Part A: Applied Science and Manufacturing*, Vol 33, issue 7, Baley C., Analysis of the flax fibers tensile behavior and analysis of the tensile stiffness increase, 2002 [22] with permission from Elsevier).

between IL and fiber mechanics, which is critical for advancing natural plant fibers in high-performance applications.

2. Materials & methods

2.1. Materials

1-ethyl-3-methylimidazolium acrylate [EMIM][ACR] was supplied by proionic GmbH (Grambach, Austria) and used without further purification and drying (for details on the ionic liquid and water content we refer to Pachernegg et al. [60]). Acetone ($\geq 99.5\%$, CarlRoth, Germany) and ethanol (99 % Rotipuran, CarlRoth, Germany) were used as received. As a reference substrate, retted and untreated European flax fibers were obtained from a commercial source, which applies the fibers in composite applications. Therefore, the fibers were assembled in bundles in a cord and prior to further treatment, single fibers were carefully extracted from the bundles.

2.2. Sample preparation

Silicon wafers (Siebert Wafers, Germany) were cleaned using acetone, ethanol, and deionized water in sequence. Post-cleaning, the wafers were dried under a nitrogen stream. A line was scratched into the surface of the silicon wafer to enable the determination of the fiber orientation in the AFM. Following the cleaning and drying of the wafer, industrial untreated, retted flax fibers were fixed onto the silicon wafers using commercial nail polish (Figure S3A) at 90° angle to the scratch. The fibers were stored in lab atmosphere prior to the treatment with the ionic liquid [EMIM][ACR] to stabilize water content of each fiber. Each fiber was treated with $40\ \mu\text{L}$ of ionic liquid (manipulation at room conditions 22°C , 50% RH), which results in a local treatment. The partially immersed fibers were, immediately after IL application, stored in a desiccator for 15 min, 30 min, 45 min, 1 h, 7 h and 24 h, respectively. After treatment, the wafers were washed in a stream deionized water using a wash bottle. To remove residual ionic liquid, the fibers were subsequently immersed in water for 15 min and then dried under a nitrogen stream. The untreated fibers were only subjected to the washing step.

2.3. Atomic force microscopy (AFM)

AFM images were recorded using a FastScan Bio Atomic Force Microscope (Bruker, USA) operated by a Nanoscope V controller. Silicon cantilevers (AP-ARROW-NCR from NanoWorld AG, Neuchatel, Switzerland) with a nominal force constant and tip radius of $42\ \text{N m}^{-1}$ and $<10\ \text{nm}$, respectively, were used in tapping mode. All experiments were conducted at 23°C and ambient relative humidity conditions ($30\text{--}50\%$ RH). Three individual flax fibers for each treatment were investigated with $5 \times 5\ \mu\text{m}^2$ topography scans at three individual positions on the fiber. Image processing was performed using Gwyddion v2.58 software. A detailed description of the determination of the microfibril angle (MFA) and microfibril (bundle) diameter data is provided in section S2 of the Supporting Information (SI). As presented in Fig. 2, a positive microfibril angle corresponds to a clockwise orientation of the microfibrils whereas a negative MFA is counterclockwise. Average values, of the microfibril (bundle) angle, were determined from the absolute values independent of counter- or clockwise orientation. Furthermore, the full two-dimensional power spectral density function (2D PSDF) of the AFM topography images was obtained to evaluate characteristic spatial frequencies occurring on the differently treated samples – as another measure of the local MFA distribution.

2.4. Wide-angle X-ray scattering (WAXS) and MFA determination using WAXS and microtome data

Wide-angle X-ray scattering (WAXS) measurements were performed

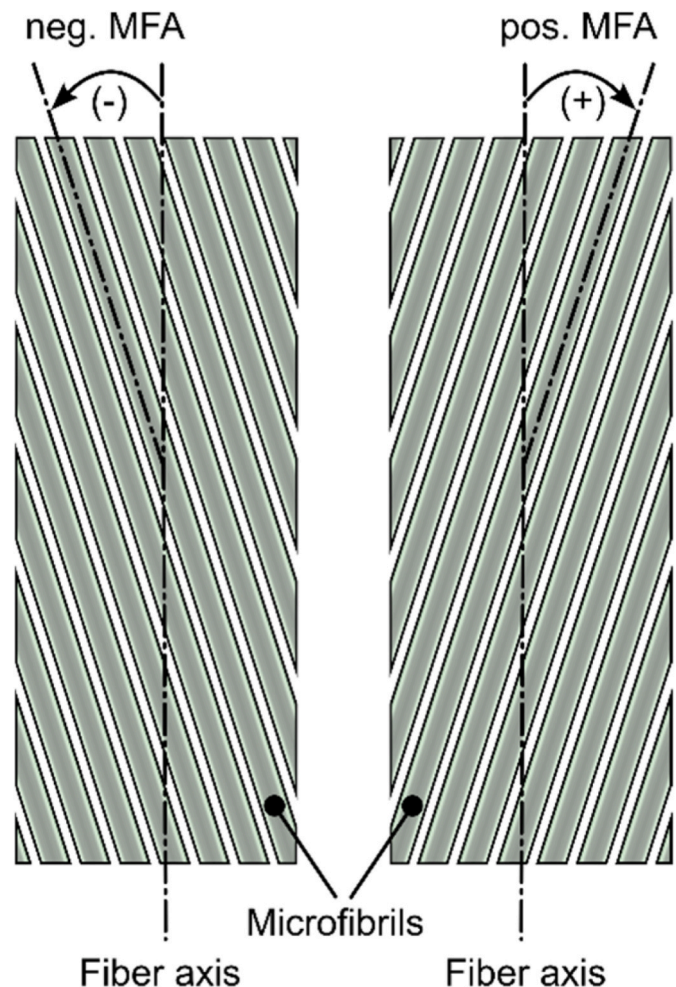


Fig. 2. The MFA determined from AFM was counted negative if the microfibril orientation was counterclockwise. Whereas the clockwise direction corresponds to a positive MFA.

on three individual single flax fibers with a SAXSpoint5.0 instrument (Anton Paar, Austria). For each fiber, 22 frames with an acquisition time of 300 s were obtained. The sample-detector distance was 64.2 mm, and the beam diameter was 2.4 mm. Cu K α radiation with a wavelength of 0.154 nm was used with the (200)-peaks of cellulose appearing for the flax fibers at $2\theta \sim 22.6^\circ$. The fibers were measured in an evacuated chamber with the long axis of the fiber in a horizontal arrangement. For the data processing, the software “SAXSanalysis” of Anton Paar was used.

The MFA was determined from the WAXS data and the cell wall orientation using the method described by Rüggeberg et al. [61]. The method predicts measured intensity as a function of azimuthal angle, cell wall orientation and MFA. The intensity, azimuthal angle and cell orientation are known quantities provided by the experiments. The MFA is found by solving the inverse problem using error minimization. In this work, a single fiber is imaged at a time, which is different from the experiment on longitudinal tissue sections done by Rüggeberg et al. [61], but in practice works the same way as when imaging several fibers. The cell wall orientation is obtained after WAXS measurement along the length of the fiber from the microtome cross-sections of the fibers.

Each fiber was embedded in a glycol methacrylate resin and left to cure for 24h. Afterward, the embedded sample was placed in a microtome and cut at ten different positions along the length of the fiber. For the flax fibers, this means that every $400\ \mu\text{m}$ along their length a cross-sectional image was recorded [62]. Since these fibers are rather uniform and show little deviation in their cross-section, this distance seemed

appropriate. In general, flax fibers exhibit a rather uniform cross-section with a small lumen.

To determine the orientation of the cell wall relative to 90° of the incoming X-ray beams, all cross-sectional images were analyzed according to Fig. 3. The cell wall was separated into parts with the same orientation angle and their length was measured in pixel. This analysis was performed using ImageJ (NIH, USA). Since the flax fibers were spanned across the whole length of the sample holder and glued at both ends to it, the chance that a misalignment happened between the WAXS measurement, and the microtome cutting is very small. Only the embedding procedure could slightly alter the orientation, however, care was taken to keep the fiber as straight as possible in the embedding capsule.

By combining the microtome data and WAXS measurements the azimuthal intensity profile of the (200)-peak could be effectively modeled by the sum of a constant term (random orientation of cellulose microfibrils), and two Gaussian distributions. This is similar to the number of unknowns as in the work of Rüggeberg et al. [61]. There are seven unknown fitting parameters: The amplitude of the random distribution and the mean, standard deviation, and amplitude of the two Gaussian distributions. The seven unknown fitting parameters are found by error minimization so that the model output matches the measured output. A detailed description of the model and the implementation is given in the literature [61].

2.5. Tensile testing

Tensile testing of the single treated (1h and 24h) and reference flax fibers was performed with displacement-controlled ramps until breakage with a displacement rate of 10 µm/s in a dynamic mechanical analyzer (DMA 850, TA Instruments, USA) at controlled relative humidity and temperature conditions (50 % RH, 23 °C). The span length of the single fibers was 8 mm. Afterward, each individual fiber was microtome cut at three different positions according to the procedure reported by Zizek et al. [62] and the average cross-sectional area evaluated to obtain the proper stress values for each flax fiber.

Altogether, 43 fiber samples were tested (8 reference, 21 1h treatment, 14 24h treatment).

2.6. Brillouin spectroscopy

Brillouin spectroscopy was applied to three individual reference flax fibers and two different flax fibers after 24h treatment. The setup is described in detail in the literature by Czibula et al. [58,63]. The relative humidity (RH) varied between 30 % and 50 % RH whereas the room temperature was maintained at 20°C–21 °C. A 532 nm laser is used in combination with a scanning Tandem Fabry-Pérot interferometer (TFP-1, TableStable Ltd., Switzerland) applying the 90a-scattering geometry to measure the signal along the axial axis of the fibers. All fibers were aligned in such a way that measurements were performed in the

axial fiber direction. Polarizers in different alignments (HH – parallel, HV – crossed) were used to identify the longitudinal and transverse phonon modes, respectively.

In Brillouin scattering, the laser light is inelastically scattered from acoustic phonons in the material [51]. From measurements of a material, one obtains a spectrum which exhibits peak doublets (Stokes and Anti-Stokes) which are frequency-shifted by several GHz from the Rayleigh peak. Peaks are fitted with Lorentzian functions to identify the frequency shift, Δf , of the Brillouin scattered light. The Δf is related to the sound velocity, V , via the refractive index, n , of the material, the incident laser wavelength λ , and the scattering geometry, θ .

$$\Delta f = \pm \frac{nV}{\lambda} \sin \frac{\theta}{2} \quad (\text{Equation 1})$$

By using an equal-angle 90a-scattering geometry, the equation to obtain the sound velocity V is:

$$V = \frac{\Delta f \lambda}{\sqrt{2}} \quad (\text{Equation 2})$$

From there, the calculation of stiffness values C_{ij} needs consideration of the density of the material ρ :

$$C_{ij} = V^2 \rho \quad (\text{Equation 3})$$

Therefore, the frequency shift obtained from the Brillouin spectrum is directly related to the elastic stiffness of the material and by knowing the symmetry of the material, one can determine the full diagonal of the elastic stiffness tensor. For a fibrous material, which is an anisotropic material and exhibits directional dependence in mechanical and optical properties, a hexagonal symmetry is commonly assumed in literature [58]. By measuring the axial direction of the flax fibers in this work, it is possible to obtain information on the normal stiffness C_{33} in the axial direction and the shear stiffness C_{44} (see Refs. [52,54,58] for more details). Since C_{44} directly corresponds to the shear modulus G_{13} , Brillouin spectroscopy enables non-contact access to fiber shear properties: $G_{13} = C_{44}$. Furthermore, in axial fiber direction, the transverse phonon modes are degenerated since their sound velocities coincide.

3. Results and discussion

3.1. Surface morphology and microfibril angle (MFA) evolution by AFM

To investigate the effect of the [EMIM][ACR] treatment on the morphology of the flax fibers, atomic force microscopy (AFM) was employed and several fibers (three for each treatment) were investigated with $5 \times 5 \mu\text{m}^2$ topography scans at three individual positions on the fiber. In Fig. 4, for the untreated reference and the different treatment steps, representative topography scans are summarized. Further topography images and details are presented in section S3 of the SI. It was not possible to treat the same fiber at different time steps, but the presented

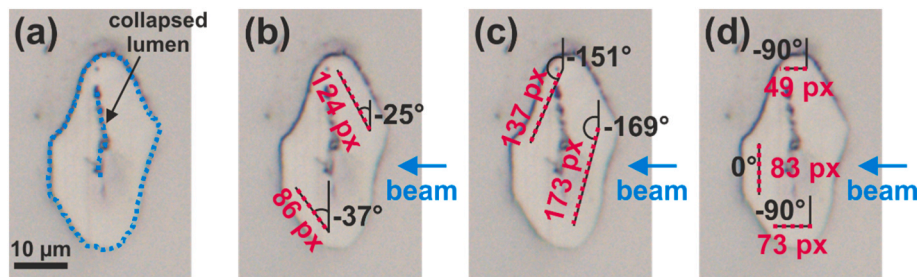


Fig. 3. (a) One cross-sectional image of a single flax fiber with a collapsed lumen. The outline and the lumen of the fiber is marked with a blue dotted line. (b)–(d) Procedure to analyze the orientation of all cell wall parts of the single fiber which show a clear difference in alignment relative to 90° of the incoming beam. For each of these cell wall parts, the length in pixels was determined as well. Altogether, the fiber cross-section presented in (a) consists of seven cell wall parts. (For interpretation of the references to colour in this figure legend, the reader is referred to the Web version of this article.)

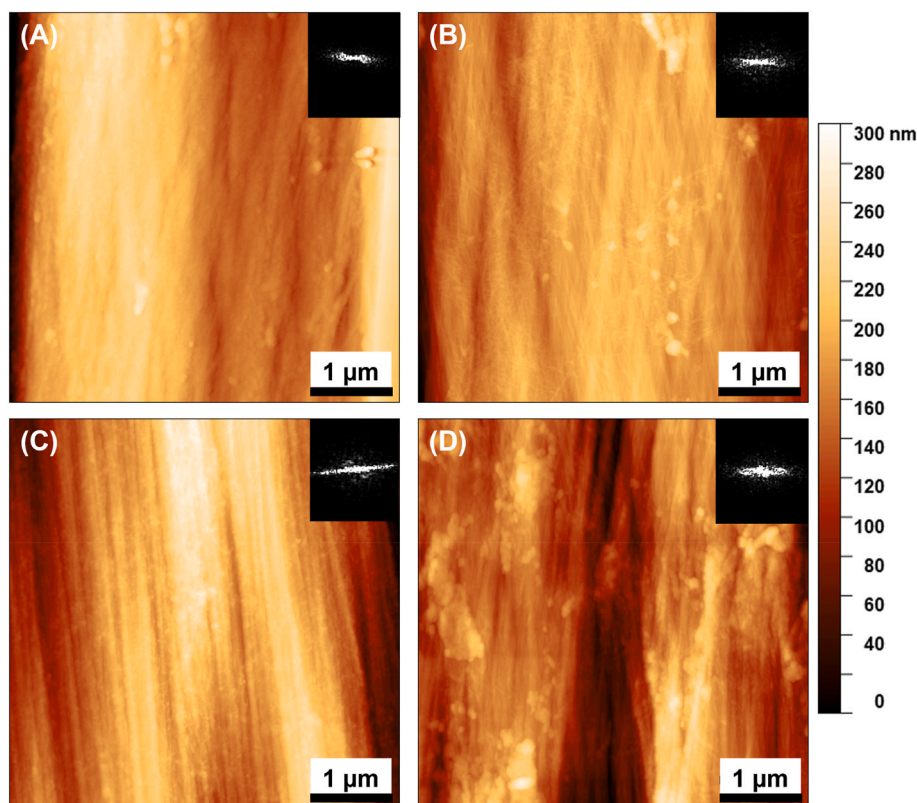


Fig. 4. Overview of $5 \times 5 \mu\text{m}^2$ representative AFM topography images of untreated and [EMIM][ACR] treated flax fibers (z-scale: 300 nm). In (A), an untreated flax fiber and in (B)–(D), flax fibers after different treatment times with [EMIM][ACR] are presented: (B) after 1h treatment, (C) after 7h treatment, and (D) after 24h treatment. The insets in each image represent the 2D PSDF indicating preferred orientation of the fiber surface. In (C), the predominant direction is clearly indicated at an angle of 5.6° , which corresponds well with the measured MFAs.

results were obtained from different flax fibers of the same batch.

In general, native, untreated flax fibers typically show a wrinkled surface, which exhibits no clear alignment of microfibril (bundles) as reported in the literature [32,64], which is also observed for our samples. This is clearly indicated in the representative Fig. 4 (A). When the fibers are separated from the plant by mechanical treatment, the primary layer is the outmost layer, which might have suffered some damage due to the treatment or exhibits surface contaminations. These surface contaminations cannot be removed even after extensive rinsing with water (see Table S1 in SI).

After treatment of the fiber for 1h with [EMIM][ACR] a fine fibril structure on the surface of the fibers from the AFM topography scans appears, which does not show fully homogeneous orientation, as presented in Fig. 4 (B). The width of the microfibril (bundles) (averaged from 47 measurement points) was 95 ± 50 nm. Since these values are higher than those expected for individual microfibrils (usually in the range of <5 nm, and hardly accessible by AFM) [22,65–69], we argue that the observed features on the surface are bundles or aggregates of these microfibrils (so-called macrofibrils). The size range expected for such features depends on the plant species. The values reported are between 10 and 60 nm for fibers derived from trees [32,66,70,71] while values up to 100 nm are reported for flax fibers [65]. These large aggregates may also be caused by the removal of pectin and hemicellulose [34,72–74]. Despite the fact, that these agglomerations may alter the measured values, they are still highly oriented and can be used to determine the MFA [75–77].

At some positions, almost horizontally distributed fibril bundles are distinguishable, which may represent fractions of the primary wall or the S1 layer of the cell wall (see Table S2 in SI). Increasing the treatment time to 7h with [EMIM][ACR] leads to the complete dissolution of the top layers of the cell wall (Fig. 4 (C)), and consequently, a highly

structured surface corresponding to the S2 layer is obtained [30]. The alignment of microfibril bundles is close to the axial fiber direction and the fibril diameter, obtained from the AFM topography images, corresponds to 90 ± 30 nm. These values correspond to the typical range of bundles of cellulose microfibrils in flax [32,33,65,78]. Furthermore, by determining the orientation of these microfibril bundles from the AFM scans (see SI for further details), an MFA of $5.7 \pm 1.9^\circ$ was determined. This agrees well with the results obtained by WAXS analysis (see section S1, Fig. S1 in SI). The insets in Fig. 4 represent the 2D power spectral density function (PSDF) of each image and show only for the 7 h treatment a distinct orientation at an angle of 5.6° , which is another confirmation of a good agreement between the local AFM results from the S2 layer and the averaging WAXS measurement of the full fiber.

After 24 h of exposure to [EMIM][ACR], little changes in morphology are observed as presented in Fig. 4 (D). Most notably, there are additional agglomerates (areas of undefined fiber structure) on the surface of the fiber visible compared to shorter exposure times to the IL, which causes the loss of the distinct orientation in the 2D PSDF. Based on atomic force microscopy (AFM) scans, no phase contrast was detected, indicating that these agglomerates are components of the fiber itself. Their precipitation onto the surface may be influenced by the treatment conditions used in this study.

All the IL-treatments were performed on the single fiber level with each fiber glued by nail polish to a silicon wafer. The removal of the IL containing dissolved flax fiber compounds from the primary wall, the S1-layer and parts of the S2-layer cannot be done with water as anti-solvent in a suitable timeframe to minimize reprecipitation. Especially as the viscosity of the IL solution is strongly increased by the dissolved components, it gets complicated to remove the solution efficiently [79, 80] without changing the fibers properties. This results in an irregular surface with additional agglomerations, which are most likely a direct

result of the treatment and no direct statement can be made if these agglomerates would also precipitate on the fiber surface in a different procedure setting.

Although flax fibers are often used as reference materials due to their homogeneity, they are still a natural material and exhibits variability in their properties and structural features. In Fig. 5, the distribution of the MFA and fibril bundle diameter for the investigated fibers are summarized. With increasing treatment time, the scattering of the data is reduced, which indicates that the heterogeneity of the surface decreases. Due to its high degree of alignment of the microfibrils, and subsequently the microfibril bundles, the highest degree of homogeneity is expected for the S2 layer, which is visible in the AFM images after the 7h treatment (Fig. 4 (C)). This trend is confirmed by the 2D PSDF insets of the AFM topography images in Fig. 4. Only in Fig. 4 (C), a clear preferred direction of orientation is observable, which matches the MFA. Untreated flax fibers were also investigated for their microfibril (bundle) angle distribution by WAXS to determine the MFA. In general, WAXS is capable to compensate for the inhomogeneities of the fiber matrix, which are considered as defects. In our paper, the procedure described by Rüggeberg et al. [61] was adapted to the single fiber level. In Figure S1 (A) in the SI, the WAXS patterns for three different flax fibers are presented. From the three fibers, an MFA value of $(5.0 \pm 1.6^\circ)$ (Figure S1 (B)) was determined. The values obtained are similar to literature values as presented in Table 1, with some variations depending on the origin and pre-treatment of the flax fibers. Furthermore, the results from WAXS and AFM in this work are in agreement.

The evaluation of the MFAs of the untreated, reference flax fibers with AFM reveals a broad distribution of the MFA ranging from nearly -20° to almost 30° (Fig. 5 (A), green rectangles). When determining the angles from the AFM images (see for details in the Materials and Methods section and the SI) the negative sign implies a counter clockwise orientation of the microfibril bundles. Since for untreated fibers mostly the primary wall is exposed, which is mainly composed of somewhat randomly distributed microfibrils (and their bundles) [30,

Table 1

Microfibril angles of flax fibers from the literature compared to this work.

	Microfibril angle/ $^\circ$	Technique
Richely et al. [81]	6.6 ± 0.5	WAXS
Bourmaud et al. [48]	8.3–9.5	WAXS
Müller et al. [82]	± 3.5	SAXS
Müller et al. [83]	5.3–6.4	SAXS
Wang et al. [84]	6.2–7.2	WAXS
Wang et al. [84]	5.8–7.3	SEM
This work	5.7 ± 1.9^a	AFM (7h IL treatment)
This work	5.0 ± 1.6	WAXS (non-treated)

^a Microfibril bundle angle.

32], a high degree of variation is expected (this work: -10° – 13°). The same is true for the microfibril bundle diameter (90–270 nm). The broad distribution of microfibril bundle diameters can either be the result of an agglomeration of individual bundles to form larger clusters or the presence of thicker microfibril bundles on the surface of the fiber. Also, the intact matrix (hemicellulose, pectin) makes it more complex to distinguish between individual microfibril bundles on the surface. Furthermore, the finite size of the AFM tip can influence the width of scanned features, especially if the tip picks up contaminations, which often happens when measuring biological materials [85,86].

The treatment of the fibers with the ionic liquid [EMIM][ACR] for 1h leads to a narrower distribution of the MFA and microfibril bundle diameter (55–145 nm). The treatment decreases the maximum microfibril bundle diameter from 400 nm down to around 200 nm. Similarly, the MFA distribution shows less variation (-8° – 12°). Nonetheless, there are still microfibril bundles oriented in both, clockwise and counter-clockwise direction, suggesting that after 1h of treatment the primary wall is removed, but the S1 layer is still partially or even fully intact. This is also confirmed by the AFM topography scans, which still show fractions of differently oriented layers (see Fig. 4 (B) and Table S2 in section S3 of the ESI [30,31]).

After 7h of IL treatment, the MFA values determined from the AFM

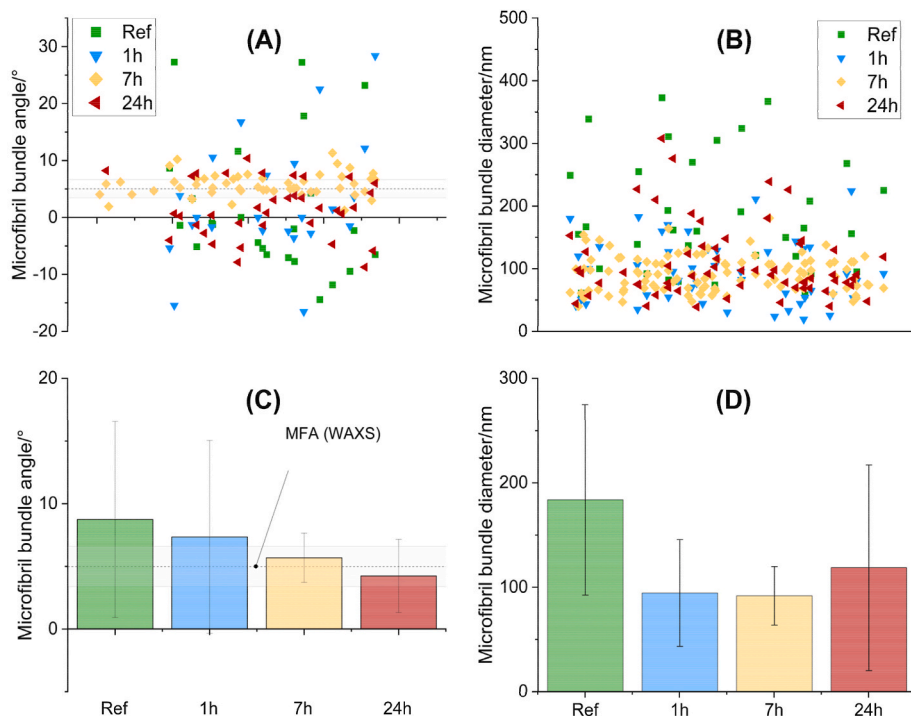


Fig. 5. (A) Single measurement points of the microfibril angle (MFA) in degrees from AFM topography images with the marked range (light grey dashed line) of MFA as determined by WAXS and (B) the microfibril bundle diameter values in nanometer as determined from AFM topography images. (C) Average microfibril bundle angle (MFA) with its variation calculated from the absolute values (dashed grey line indicates the MFA results from WAXS) and (D) microfibril bundle diameter with its variation. All data was measured from the captured AFM images of the flax fibers at different treatment times.

images reveal a uniform distribution ranging between 0° and 10° (only clockwise distribution). Similarly, the range of the microfibril bundle diameter goes down to values between 50 nm and 150 nm. The MFA values are in close correlation with the data obtained with WAXS for flax fibers, as presented in Table 1.

After a treatment of 24h comparatively higher values of MFA and microfibril bundle diameter are observed. This indicates that the dissolution process is starting to affect also the morphology of the S2 layer. As observed in Fig. 4 (D), agglomerates precipitated on the surface of the fiber, which result in a loss of the clear orientation in the 2D PSDF and, therefore, increases also the uncertainty of the MFA determination again (see Fig. 5 (C)). The agglomerates appear to be components of the fiber itself since AFM scans provided no clear phase contrast. Furthermore, the increase of the microfibril bundle diameter is also affected by the agglomeration on the fiber surface and also by further agglomeration of the microfibrils due to the treatment [87–91]. Fig. 5 (D) shows an increase and higher scattering of the diameter values of the microfibril bundles. Furthermore, the agglomerates could also cause tip contamination, which would result in a broadening of measured surface features.

Overall, the MFA values of the AFM analysis obtained for the 7h treatment is matching the WAXS results best, which indicates that the S2 layer was exposed by the treatment. Prolonged treatment (>7h) might cause damage to the S2 layer affecting the mechanical performance of the fibers, which can be assessed by mechanical testing.

3.2. Mechanical characteristics at different frequency regimes

Tensile testing was performed on single fibers of the untreated, 1h and 24h treated flax fibers to see if effects of the IL treatment on the mechanical behavior of the fibers can be determined. The 1h and 24h treatment times were specifically chosen to represent two critical points: short-term exposure (1h) and a condition of prolonged interaction of the fiber with the ILs to gain statistically significant information (24h). In Fig. 6, the results of these tests are summarized, with Fig. 6(A)–(C)

showing the stress-strain diagrams and Fig. 6 (D) illustrating the Young's moduli in a boxplot. Results for untreated flax fibers agree with literature values [22,81,92]. With increasing treatment time, the Young's modulus is decreasing. In Table 2, the mechanical parameters – tensile strength, elongation at break, and Young's modulus – obtained from tensile testing are summarized.

The untreated flax fibers exhibit an average Young's modulus of about 36 GPa. After 1h, the mean value is at 32 GPa, and after 24h of treatment, the Young's modulus drops to 22 GPa. Furthermore, the high scattering, which is common for natural fibers, is significantly reduced. A similar trend is observable for the tensile strength, which drops from around 700 MPa to about 350 MPa after 24h of treatment. A similar decrease in tensile strength was also found for hemp and bamboo fibers, which were exposed to a thermal treatment [17]. Only for the elongation at break, no significant effect is observed as a function of exposure time to the IL. The strong decrease of the tensile strength suggests the partial dissolution of the flax fiber cell wall, and especially the S2 layer, since it is the major contributor to the mechanical strength of cellulose fibers [93]. Initially, as witnessed by AFM, only the outer layer of the fibers, which contain a high percentage of lignin, hemicelluloses, and pectin are dissolved. Therefore, no significant decrease in strength can be detected for the flax fibers. Different mechanisms contribute to a

Table 2

Overview of the mechanical parameters – tensile strength, elongation at break, and Young's modulus – obtained by tensile testing for untreated, reference flax fibers ($n = 8$), and flax fibers treated for 1h ($n = 21$) and 24h ($n = 14$). The values are presented as mean value \pm 95 % confidence interval.

Flax fibers	Tensile strength/ MPa	Elongation at break/ %	Young's modulus/ GPa
Untreated	680 ± 240	3.3 ± 1.0	36.2 ± 7.1
1h treated	530 ± 130	2.5 ± 0.4	31.5 ± 5.3
24h treated	370 ± 60	3.1 ± 0.5	21.7 ± 3.1

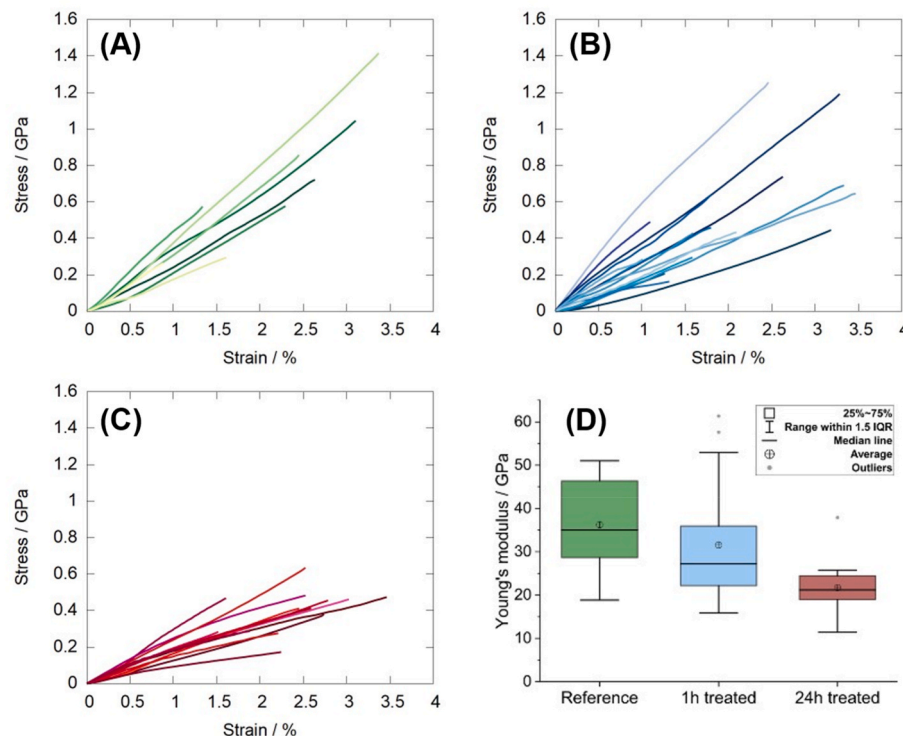


Fig. 6. Stress-strain diagrams for (A) untreated, (B) 1h treated, and (C) 24h treated flax fibers from tensile testing. (D) Boxplot of the results for the Young's modulus of the untreated (8 fiber samples), 1h (21 fiber samples) and 24h (14 fibers samples) treated flax fibers.

strength loss in longitudinal direction. It is possible that the [EMIM] [ACR] attacks the regions of dislocated cellulose connecting the nanocrystals to nanofibrils, which directly reduces their longitudinal stiffness [94]. Also, dissolution of the hemicellulose surrounding the nanofibrils is a possible mechanism as this leads to increased slippage of the nanofibrils under tensile load [95,96]. The analysis of fiber mechanics with Brillouin spectroscopy will help to understand the results of the tensile tests.

3.3. Brillouin spectroscopy

In addition to the tensile testing, Brillouin spectroscopy was applied to study untreated and 24 h treated flax fibers in axial fiber direction. Since it is an optical technique, it enables non-contact measurement of the fibers and gives different information than standard tensile testing. A 90a-scattering geometry was applied to measure directly along the axial direction of the flax fibers and in Fig. 7, representative spectra are presented. Since we measured in the axial fiber direction and the flax fiber can be considered hexagonally symmetric (see Materials and

Methods section), this measurement will give not only information on the axial stiffness of the fiber but also the shear stiffness of the fiber. Here, it should be noted that Brillouin spectroscopy has a resolution in the μm -range [97], depending on the applied optics and investigated material, therefore, the spectra measured for the untreated sample will be an average of several cell wall layers, but dominated by the S2 layer, whereas the spectra of the 24 h treated sample, will average over the S2 layer mostly. In Fig. 7 (A), Brillouin spectra are presented, in which the fibers were measured employing two parallel polarizers in the optical path (one before the sample, the other one before the spectrometer). In this HH-alignment, only longitudinal phonon modes (which correspond to the peaks highlighted in the shaded area) are detected and they give information on the normal stiffness in the axial fiber direction (C_{33}). Comparing the peaks for the untreated and 24h treated shows that there is little variation between these peaks, which can be caused by natural variations of the fibers. A frequency shift of (15.2 ± 0.3) GHz was obtained for the untreated flax fibers, whereas for the 24h treated flax fibers the value is (14.0 ± 0.3) GHz. This corresponds – by assuming a flax fiber density of 1450 kg/cm^3 [49,92] – to stiffness values of 47 GPa

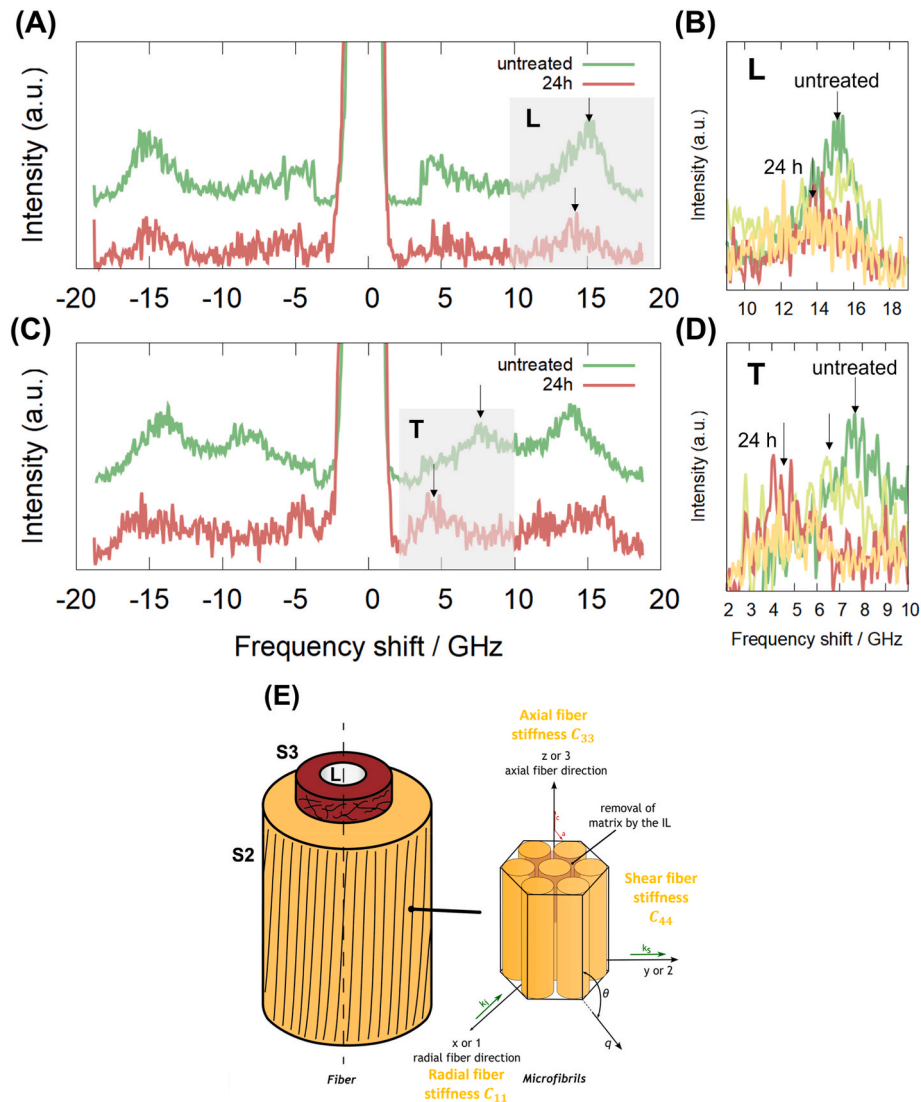


Fig. 7. Representative Brillouin spectra of the untreated and 24h treated flax fibers. In (A) HH-polarizer alignment to identify the longitudinal phonon modes with (B) as the corresponding zoom-in of the grey shaded area of interest including a second spectra for each treatment. In (C) HV-polarizer alignment to detect the transverse phonon modes. Please note that here the longitudinal mode is leaking in due to its mixed-mode nature. In (D) the corresponding zoom-in of the grey shaded area of interest in (C) is presented including a second spectra for each treatment. (E) Schematic representation of the fiber and the measurement approach of Brillouin spectroscopy. k_i and k_s correspond to the incident and scattered laser beam, respectively, whereas q indicates the direction of the probed phonons. The fiber can be assumed to have hexagonal symmetry and coordinates $[x,y,z | 1 = 2, 3]$ illustrate the different stiffness directions.

(untreated) and 40 GPa (treated). For crystalline cellulose, stiffness values above 100 GPa are obtained from theoretical calculations [98]. In contrast, Brillouin spectra are obtained at a very high frequency regime (GHz), where the measurement is averaging across several μm of material. Therefore, mechanical information from the presented Brillouin spectra can be considered as a mix of crystalline and amorphous fiber compounds and reflect their mechanical behavior in the GHz regime. Additionally, it is important to point out that these stiffness values are C_{33} and not the Young's moduli of the single fiber, the whole stiffness tensor needs to be evaluated for that relation [52,54,58]. Therefore, one should be careful in further interpretation. For the shear properties, this is much easier, although the transverse phonon peaks are trickier to measure. In Fig. 7 (C), the same fibers as in Fig. 7 (A) were measured at the identical position, however, here the polarizers were crossed (HV). This results in only detecting transverse phonon modes. However, in heterogeneous materials like natural fibers, it is very common that the longitudinal peak still appears because it is actually a mixed mode [58, 99]. In the shaded area of Fig. 7 (C), the transverse mode of the untreated and 24h treated flax fiber is highlighted and here, a clear difference in frequency shift is visible. The value decreases from (7.6 ± 0.5) GHz (untreated) to (4.8 ± 0.5) GHz (24h treated), which corresponds to shear modulus values of 12.0 GPa and 4.6 GPa, respectively. The shear modulus decreases by nearly a factor of three due to the IL treatment. In the literature, the shear moduli of the fiber's chemical compounds were investigated individually [100–102] and result in much lower values compared to the 12 GPa. However, here it should be once more emphasized that a direct comparison of Brillouin spectroscopy results with destructive mechanical testing is not straightforward because the material behavior is different in the GHz range compared to roughly 1 Hz for standard mechanical testing. In Fig. 7(B, D), zoom-ins of the peak regions indicated in Fig. 7 (A, C) are presented including spectra from two different fibers per treatment.

It is important to understand that Brillouin spectroscopy measures a high frequency response of the material (GHz). Therefore, the flax fiber, which is a viscoelastic material, will have a different mechanical response during Brillouin measurements compared to the tensile tests, which operates in the Hz regime. During single fiber tensile testing not only the fast response of nanofibril longitudinal stiffness is observed, but also the much slower process of shear failure of the matrix connecting the fibrils is contributing to the longitudinal extension of the fiber. As discussed above, both parts – the stiffness of the fibrils [94] and the slippage of the fibrils in the hemicellulose matrix [95,96] – are contributing to the longitudinal stiffness and strength of the fiber. The Brillouin results are explaining the causes for the strength decrease of the fibers due to the [EMIM][ACR] treatment. The Brillouin normal stiffness is dominated by the mechanical response of the stiff, reinforcing microfibrils along the fiber axis (Fig. 7 (E)). Their stiffness is only dropping from 47 GPa to 40 GPa after the treatment, suggesting that the nanofibrils were not strongly affected by the ionic liquid. The effect of the matrix is observable in the Brillouin shear stiffness of the fiber, since the shear deformation of composites in direction of the reinforcement are dominated by the matrix properties (Fig. 7 (E)). Here, a clear decrease of the shear modulus is observed (from 12.0 GPa to 4.6 GPa), which indicates that the IL treatment is affecting the hemicellulose matrix considerably. Comparing Fig. 4(C) and (D) of the AFM scans support this interpretation. The microfibril structure stays intact even after a treatment of 24h, whereas the agglomerations on the surface of the fiber could indicate the removal of matrix material. In summary, the results from Brillouin spectroscopy confirm that the drop in fiber stiffness due to the [EMIM][ACR] treatment is mainly caused by a degradation of the hemicellulose and pectin matrix in the fibers, and to a lesser extent by a degradation of the microfibrils.

4. Conclusions

In this study, we have used a combined methodology using wide-

angle X-ray scattering (WAXS), atomic force microscopy (AFM), tensile testing, and Brillouin spectroscopy to investigate the effects of the IL ([EMIM][ACR]) on flax fibers. This approach enables characterization of the structural and mechanical evolution of fibers during selective dissolution.

The controlled dissolution process using [EMIM][ACR] selectively removes the primary wall and S1 layer, providing direct access to the mechanically dominant S2 layer. AFM and WAXS measurements of microfibril angles (AFM: $5.7 \pm 1.9^\circ$; WAXS: $5.0 \pm 1.6^\circ$) are in agreement, validating this approach for structural characterization. Tensile testing reveals a reduction in Young's modulus (from 36 GPa to 22 GPa) and tensile strength (by a factor of 2) with increasing treatment time, highlighting the influence of hemicellulose and pectin removal on fiber mechanics.

Brillouin spectroscopy reveals a significant decrease in shear modulus (G_{13} : 12.0 GPa–4.6 GPa) caused by matrix degradation, while the normal stiffness (C_{33}), dominated by crystalline cellulose, remains largely unaffected. AFM imaging confirms intact microfibril structures, supporting our hypothesis that dissolution primarily affects non-cellulosic components in the layers visible. Furthermore, the results are demonstrating that the shear strength of the hemicellulose matrix is highly relevant for the tensile strength of the fiber. This clearly shows in the fiber's response towards different time scales in testing (tensile testing Hz-regime, Brillouin spectroscopy GHz regime).

Together, these findings showcase that the ionic liquid treatment predominantly disrupts the matrix components, affecting structural integrity and the mechanical properties of the fibers. This combined methodology provides a robust framework for studying the interplay between structure and mechanics in natural fibers undergoing chemical treatments.

Next, the underlying mechanisms of how the ionic liquid interacts with the fiber, especially the matrix components, needs to be addressed at the molecular level. Here, adapting atomic force microscopy in combination with infrared spectroscopy to the fiber scale will yield local chemical information, which can be connected with the topographical changes as well. Additionally, also effects of impurities, such as water, should be studied in such a context to get a better understanding on how changes of the ionic liquid effects mechanical properties.

CRedit authorship contribution statement

Lukas Pachernegg-Mair: Writing – review & editing, Writing – original draft, Visualization, Methodology, Investigation, Formal analysis, Data curation, Conceptualization. **Jana B. Schaubeder:** Writing – review & editing, Writing – original draft, Visualization, Validation, Methodology, Investigation, Formal analysis, Data curation, Conceptualization. **August Brandberg:** Writing – review & editing, Writing – original draft, Visualization, Validation, Software, Methodology, Investigation, Formal analysis, Conceptualization. **Michael Thoman:** Writing – review & editing, Investigation, Data curation. **Georg Urstöger:** Writing – review & editing, Methodology, Investigation. **Markus Rüggeberg:** Writing – review & editing, Validation, Software, Methodology, Formal analysis. **Kristie J. Koski:** Writing – review & editing, Validation, Resources, Methodology. **Harald Plank:** Writing – review & editing, Resources, Methodology. **Ulrich Hirn:** Writing – review & editing, Supervision, Funding acquisition. **Stefan Spirk:** Writing – review & editing, Supervision, Funding acquisition. **Caterina Czibula:** Writing – review & editing, Writing – original draft, Validation, Supervision, Methodology, Investigation, Funding acquisition, Conceptualization.

Data availability statement

The data presented in this article is shared via a repository with a DOI link. Czibula, C., Pachernegg-Mair, L., & Schaubeder, J. (2025). Ionic liquid treatment of flax fibers and the effects on morphology and

mechanical properties [Data set]. Graz University of Technology. <https://doi.org/10.3217/tw84q-2bj05>.

Declaration of generative AI and AI-assisted technologies in the writing process

During the preparation of this work the authors used ChatGPT 4o (OpenAI, USA), Perplexity.AI (USA) and Scite.ai (USA) in order to enhance readability, language and search efficiently for scientific data. After using these tools/services, the authors reviewed and edited the content as needed and take full responsibility for the content of the publication.

Declaration of competing interest

The authors declare the following financial interests/personal relationships which may be considered as potential competing interests: Lukas Pachernegg-Mair, Stefan Spirk, Ulrich Hirn reports financial support was provided by Austrian Research Promotion Agency. Caterina Czibula reports financial support was provided by Austrian Science Fund. Caterina Czibula, Michael Thoman reports financial support was provided by Office of the Styrian Provincial Government. Lukas Pachernegg-Mair, Stefan Spirk, Ulrich Hirn reports financial support was provided by European Innovation Council. If there are other authors, they declare that they have no known competing financial interests or personal relationships that could have appeared to influence the work reported in this paper.

Acknowledgements and Funding

C. C. acknowledges the Hertha Firnberg program (project no. T 1314-N) of the Austrian Science Fund (FWF), Grant DOI: 10.55776/T1314, and the Unconventional Research project “KoMME Licht” (PN-38) granted by the Styrian Government (Land Steiermark) for funding. This work has also received funding from the Austrian Research Promotion Agency (FFG) Austria on the project No. 888427 (IonFlow, L.P.-M. and S. S.) and funding from the European Innovation Council (EIC) under grant agreement No. 101115293 (VanillaFlow, L.P.-M., U. H., and S.S.). For the purpose of open access, the author has applied a CC BY public copyright licence to any Author Accepted Manuscript version arising from this submission. Markus Damm and Roland Kalb from Proionic GmbH are acknowledged for kindly supplying the ionic liquid.

Appendix A. Supplementary data

Supplementary data to this article can be found online at <https://doi.org/10.1016/j.msea.2025.148675>.

References

- [1] M. Li, Y. Pu, V.M. Thomas, C.G. Yoo, S. Ozcan, Y. Deng, K. Nelson, A. J. Ragauskas, Recent advancements of plant-based natural fiber-reinforced composites and their applications, *Compos. B Eng.* 200 (2020) 108254, <https://doi.org/10.1016/j.compositesb.2020.108254>.
- [2] M. Ramesh, K. Palanikumar, K.H. Reddy, Plant fibre based bio-composites: sustainable and renewable green materials, *Renew. Sustain. Energy Rev.* 79 (2017) 558, <https://doi.org/10.1016/j.rser.2017.05.094>.
- [3] F. Feist, M. Wagner, G. Baumann, S. Spirk, V. Biegler, Q. Jiang, T. Nypelö, A cellulosic fibre foam as a bicycle helmet impact liner for brain injury mitigation in oblique impacts, *Heliyon* 11 (2025) e40790, <https://doi.org/10.1016/j.heliyon.2024.e40790>.
- [4] E. Orzan, A. Barrio, V. Biegler, J.B. Schaubeder, A. Bismarck, S. Spirk, T. Nypelö, Foaming and cross-linking of cellulose fibers using phytic acid, *Carbohydr. Polym.* 347 (2025) 122617, <https://doi.org/10.1016/j.carbpol.2024.122617>.
- [5] H. Sixta, in: H. Sixta (Ed.), *Handbook of Pulp*, vol. 1, WILEY-VCH Verlag GmbH & Co. KGaA, Weinheim, 2006.
- [6] H. Sixta, H. Harms, S. Dapia, J.C. Parajo, J. Puls, B. Saake, H.-P. Fink, T. Röder, Evaluation of new organosolv dissolving pulps. Part I: preparation, analytical characterization and viscose processability, *Cellulose* 11 (2004) 73, <https://doi.org/10.1023/B:Cell.0000014767.47330.90>.
- [7] M. Hohegger, B. Cottyn-Boitte, L. Cézard, S. Schober, M. Mittelbach, Influence of ethanol organosolv pulping conditions on physicochemical lignin properties of European larch, *Int. J. Chem. Eng.* 2019 (2019) 1734507, <https://doi.org/10.1155/2019/1734507>.
- [8] A. Johansson, O. Aaltonen, P. Ylinen, Organosolv pulping - methods and pulp properties, *Biomass* 13 (1987) 45, [https://doi.org/10.1016/0144-4565\(87\)90071-0](https://doi.org/10.1016/0144-4565(87)90071-0).
- [9] G. Reyes, M.G. Aguayo, A. Fernández Pérez, T. Pääkkönen, W. Gacitúa, O. J. Rojas, Dissolution and hydrolysis of bleached kraft pulp using ionic liquids, *Polymer* 11 (2019) 673, <https://doi.org/10.3390/polym11040673>.
- [10] A. Roselli, M. Hummel, A. Monshizadeh, T. Maloney, H. Sixta, Ionic liquid extraction method for upgrading eucalyptus kraft pulp to high purity dissolving pulp, *Cellulose* 21 (2014) 3655, <https://doi.org/10.1007/s10570-014-0344-x>.
- [11] L.K. Hauru, M. Hummel, A.W. King, I. Kilpeläinen, H. Sixta, Role of solvent parameters in the regeneration of cellulose from ionic liquid solutions, *Biomacromolecules* 13 (2012) 2896, <https://doi.org/10.1021/bm300912y>.
- [12] M. Martín, M. Taifouris, G. Galán, Lignocellulosic biorefineries: a multiscale approach for resource exploitation, *Bioresour. Technol.* 385 (2023) 129397, <https://doi.org/10.1016/j.biortech.2023.129397>.
- [13] T.V. Doherty, M. Mora-Pale, S.E. Foley, R.J. Linhardt, J.S. Dordick, Ionic liquid solvent properties as predictors of lignocellulose pretreatment efficacy, *Green Chem.* 12 (2010) 1967, <https://doi.org/10.1039/c0gc00206b>.
- [14] M. Hummel, A. Michud, M. Tantt, S. Asaadi, Y. Ma, L.K.J. Hauru, A. Parviainen, A.W.T. King, I. Kilpeläinen, H. Sixta, Ionic liquids for the production of man-made cellulosic fibers: opportunities and challenges, in: O.J. Rojas (Ed.), *Cellulose Chemistry and Properties: Fibers, Nanocelluloses and Advanced Materials*, Springer International Publishing, Cham, 2016, pp. 133–168.
- [15] M. Aydın, H. Tozlu, S. Kemaloglu, A. Aytaç, G. Özkoc, Effects of alkali treatment on the properties of short flax fiber-poly(lactic acid) eco-composites, *J. Polym. Environ.* 19 (2010) 11, <https://doi.org/10.1007/s10924-010-0233-9>.
- [16] M. Aly, M. Hashmi, A. Olabi, K. Benyounis, M. Messery, A. Hussain, E. Abadir, Optimization of alkaline treatment conditions of flax fiber using Box-Behnken method, *J. Nat. Fibers* 9 (2012) 256, <https://doi.org/10.1080/15440478.2012.738036>.
- [17] S. Ochi, H. Takagi, R. Niki, Mechanical properties of heat-treated natural fibers, *WIT Trans. Built Environ.* 59 (2002), <https://doi.org/10.2495/HPS020121>.
- [18] M. Samanth, K. Subrahmanya Bhat, Conventional and unconventional chemical treatment methods of natural fibres for sustainable biocomposites, *Sustain. Chem. Clim. Action* 3 (2023), <https://doi.org/10.1016/j.scca.2023.100034>.
- [19] D.E. Akin, Flax – structure, chemistry, retting and processing, in: J. Müssig (Ed.), *Industrial Applications of Natural Fibres*, 2010, pp. 87–108.
- [20] A.K. Mohanty, M. Misra, L.T. Drzal, Surface modifications of natural fibers and performance of the resulting biocomposites: an overview, *Compos. Interfaces* 8 (2001) 313, <https://doi.org/10.1163/156855401753255422>.
- [21] I. Pulkkinen, K. Ala-Kaila, J. Aittamaa, Characterization of wood fibers using fiber property distributions, *Chem. Eng. Process. Process Intensif.* 45 (2006) 546, <https://doi.org/10.1016/j.cep.2005.12.003>.
- [22] C. Baley, Analysis of the flax fibres tensile behaviour and analysis of the tensile stiffness increase, *Composites Part A* 33 (2002) 939, [https://doi.org/10.1016/S1359-835X\(02\)00040-4](https://doi.org/10.1016/S1359-835X(02)00040-4).
- [23] W.H. Morrison III, D.D. Archibald, H.S.S. Sharma, D.E. Akin, Chemical and physical characterization of water- and dew-retted flax fibers, *Ind. Crops Prod.* 12 (2000) 39, [https://doi.org/10.1016/S0926-6690\(99\)00044-8](https://doi.org/10.1016/S0926-6690(99)00044-8).
- [24] J. Foulk, D. Akin, R. Dodd, C. Ulven, Production of flax fibers for biocomposites, in: S. Kalia, B.S. Kaith, I. Kaur (Eds.), *Cellulose Fibers: Bio- and Nano-Polymer Composites: Green Chemistry and Technology*, Springer Berlin Heidelberg, Berlin, Heidelberg, 2011, pp. 61–95.
- [25] J.D. Evans, D.E. Akin, W.H. Morrison, D.S. Himmelsbach, J.A. Foulk, Modifying dew-retted flax fibers by means of an air-atomized enzyme treatment, *Textil. Res. J.* 72 (2002) 579, <https://doi.org/10.1177/004051750207200704>.
- [26] L. Yan, Effect of alkali treatment on vibration characteristics and mechanical properties of natural fabric reinforced composites, *J. Reinforc. Plast. Compos.* 31 (2012) 887, <https://doi.org/10.1177/0731684112449399>.
- [27] Y. Horikawa, Structural diversity of natural cellulose and related applications using delignified wood, *J. Wood Sci.* 68 (2022), <https://doi.org/10.1186/s10086-022-02061-2>.
- [28] R.L. Pereira Oliveira Moreira, J.A. Simao, R.F. Gouveia, M. Strauss, Exploring the hierarchical structure and alignment of wood cellulose fibers for bioinspired anisotropic polymeric composites, *ACS Appl. Bio Mater.* 3 (2020) 2193, <https://doi.org/10.1021/acsabm.0c00038>.
- [29] U. Sahlberg, L. Salmen, A. Oscarsson, The fibrillar orientation in the S2-layer of wood fibres as determined by x-ray diffraction analysis, *Wood Sci. Technol.* 31 (1997) 77, <https://doi.org/10.1007/bf00705923>.
- [30] J.R. Barnett, V.A. Bonham, Cellulose microfibril angle in the cell wall of wood fibres, *Biol. Rev. Camb. Phil. Soc.* 79 (2004) 461, <https://doi.org/10.1017/s1464793103006377>.
- [31] L. Donaldson, Microfibril angle: measurement, variation and relationships - a review, *IAWA J.* 29 (2008) 345, <https://doi.org/10.1163/22941932-90000192>.
- [32] L.J. Gibson, The hierarchical structure and mechanics of plant materials, *J. R. Soc. Interface* 9 (2012) 2749, <https://doi.org/10.1098/rsif.2012.0341>.
- [33] L. Salmén, Wood cell wall structure and organisation in relation to mechanics, in: A. Gleitmann, J. Gril (Eds.), *Plant Biomechanics*, 2018, pp. 3–19.
- [34] O.M. Astley, A.M. Donald, A small-angle X-ray scattering study of the effect of hydration on the microstructure of flax fibers, *Biomacromolecules* 2 (2001) 672, <https://doi.org/10.1021/bm005643l>.

- [35] I. Sulaeva, F.G. Stepamo, I. Melikhov, D. Budischowsky, J.L. Rahikainen, A. Borisova, K. Marjamaa, K. Kruus, V.G.H. Eijssink, A. Várnai, A. Potthast, Beyond the surface: a methodological exploration of enzyme impact along the cellulose fiber cross-section, *Biomacromolecules* 25 (2024) 3076, <https://doi.org/10.1021/acs.biomac.4c00152>.
- [36] A. Melelli, F. Jamme, D. Legland, J. Beaugrand, A. Bourmaud, Microfibril angle of elementary flax fibres investigated with polarised second harmonic generation microscopy, *Ind. Crops Prod.* 156 (2020) 112847, <https://doi.org/10.1016/j.indcrop.2020.112847>.
- [37] Y. Li, J. Wang, X. Liu, S. Zhang, Towards a molecular understanding of cellulose dissolution in ionic liquids: anion/cation effect, synergistic mechanism and physicochemical aspects, *Chem. Sci.* 9 (2018) 4027, <https://doi.org/10.1039/c7sc05392d>.
- [38] A. Pinkert, K.N. Marsh, S. Pang, M.P. Staiger, Ionic liquids and their interaction with cellulose, *Chem. Rev.* 109 (2009) 6712, <https://doi.org/10.1021/cr9001947>.
- [39] M. Ghasemi, P. Alexandridis, M. Tsiannou, Dissolution of cellulosic fibers: impact of crystallinity and fiber diameter, *Biomacromolecules* 19 (2018) 640, <https://doi.org/10.1021/acs.biomac.7b01745>.
- [40] B. Kosan, C. Michels, F. Meister, Dissolution and forming of cellulose with ionic liquids, *Cellulose* 15 (2008) 59, <https://doi.org/10.1007/s10570-007-9160-x>.
- [41] A.J. Holding, A. Parviainen, I. Kilpeläinen, A. Soto, A.W.T. King, H. Rodríguez, Efficiency of hydrophobic phosphonium ionic liquids and DMSO as recyclable cellulose dissolution and regeneration media, *RSC Adv.* 7 (2017) 17451, <https://doi.org/10.1039/c7ra01662j>.
- [42] T.R. Kraemer, G. Reyes, M. Cartes, A. Mejía, O.J. Rojas, Ionic liquid interactions with cellulose and the effect of water, *Cellulose* 31 (2024) 6597, <https://doi.org/10.1007/s10570-024-06016-2>.
- [43] F. Chen, D. Sawada, M. Hummel, H. Sixta, T. Budtova, Swelling and dissolution kinetics of natural and man-made cellulose fibers in solvent power tuned ionic liquid, *Cellulose* 27 (2020) 7399, <https://doi.org/10.1007/s10570-020-03312-5>.
- [44] L. Villar, M. Pita, J. Paez, P.B. Sánchez, Dissolution kinetics of cellulose in ionic solvents by polarized light microscopy, *Cellulose* 30 (2023) 3027, <https://doi.org/10.1007/s10570-022-05036-0>.
- [45] B. Mostofian, J.C. Smith, X. Cheng, Simulation of a cellulose fiber in ionic liquid suggests a synergistic approach to dissolution, *Cellulose* 21 (2014) 983, <https://doi.org/10.1007/s10570-013-0018-0>.
- [46] Y. Zhao, X. Liu, J. Wang, S. Zhang, Effects of anionic structure on the dissolution of cellulose in ionic liquids revealed by molecular simulation, *Carbohydr. Polym.* 94 (2013) 723, <https://doi.org/10.1016/j.carbpol.2013.02.011>.
- [47] H. Du, X. Qian, The effects of acetate anion on cellulose dissolution and reaction in imidazolium ionic liquids, *Carbohydr. Res.* 346 (2011) 1985, <https://doi.org/10.1016/j.carres.2011.05.022>.
- [48] A. Bourmaud, C. Morvan, A. Bouali, V. Placet, P. Perre, C. Baley, Relationships between micro-fibrillar angle, mechanical properties and biochemical composition of flax fibers, in: *Composites Week @ Leuven and Texcomp-11 Conference*, 2013. Leuven, Belgium.
- [49] M. Le Gall, P. Davies, N. Martin, C. Baley, Recommended flax fibre density values for composite property predictions, *Ind. Crops Prod.* 114 (2018) 52, <https://doi.org/10.1016/j.indcrop.2018.01.065>.
- [50] L. Brillouin, Diffusion de la lumière et des rayons X par un corps transparent homogène, *Ann. Phys.* 9 (1922) 88, <https://doi.org/10.1051/anphys/192209170088>.
- [51] P.M. Morse, K.U. Ingard, *Theoretical Acoustics*, 927, Princeton University Press, Princeton NJ, 1986.
- [52] S. Cusack, A. Miller, Determination of the elastic constants of collagen by Brillouin light scattering, *J. Mol. Biol.* 135 (1979) 39, [https://doi.org/10.1016/0022-2836\(79\)90339-5](https://doi.org/10.1016/0022-2836(79)90339-5).
- [53] F. Palombo, C.P. Winlove, R.S. Edginton, E. Green, N. Stone, S. Caponi, M. Madami, D. Fioretto, Biomechanics of fibrous proteins of the extracellular matrix studied by Brillouin scattering, *J. R. Soc. Interface* 11 (2014) 20140739, <https://doi.org/10.1098/rsif.2014.0739>.
- [54] K.J. Koski, P. Akhenblit, K. McKiernan, J.L. Yarger, Non-invasive determination of the complete elastic moduli of spider silks, *Nat. Mater.* 12 (2013) 262, <https://doi.org/10.1038/nmat3549>.
- [55] D.R. Williams, D.J. Nurco, N. Rahbar, K.J. Koski, Elasticity of bamboo fiber variants from Brillouin spectroscopy, *Materialia* 5 (2019) 100240, <https://doi.org/10.1016/j.mtla.2019.100240>.
- [56] Y. Zhang, B.W. Reed, F.R. Chung, K.J. Koski, Mesoscale elastic properties of marine sponge spicules, *J. Struct. Biol.* 193 (2016) 67, <https://doi.org/10.1016/j.jsb.2015.11.009>.
- [57] H. Keshmiri, D. Cikes, M. Samalova, L. Schindler, L.-M. Appel, M. Urbanek, I. Yudushkin, D. Slade, W.J. Weninger, A. Peaucelle, J. Penninger, K. Elsayad, Brillouin light scattering anisotropy microscopy for imaging the viscoelastic anisotropy in living cells, *Nat. Photonics* 18 (2024) 276, <https://doi.org/10.1038/s41566-023-01368-w>.
- [58] C. Czibula, M.H. Ulz, A. Wagner, K. Elsayad, U. Hirn, K.J. Koski, The Elastic Stiffness Tensor of Cellulosic Viscose Fibers Measured with Brillouin Spectroscopy, vol. 6, *JPhys Photonics*, 2024 035012, <https://doi.org/10.1088/2515-7647/ad4cc6>.
- [59] K. Elsayad, G. Urstöger, C. Czibula, C. Teichert, J. Gumulec, J. Balvan, M. Pohl, U. Hirn, Mechanical Properties of cellulose fibers measured by Brillouin spectroscopy, *Cellulose* 27 (2020) 4209, <https://doi.org/10.1007/s10570-020-03075-z>.
- [60] L. Pachernegg, J. Maier, R. Yagmur, M. Damm, R. Kalb, A.M. Coclite, S. Spirk, Physicochemical properties of 20 ionic liquids prepared by the carbonate-based IL (CBILS) process, *J. Chem. Eng. Data* 69 (2024) 1814, <https://doi.org/10.1021/acs.jced.3c00687>.
- [61] M. Rüggeberg, F. Saxe, T.H. Metzger, B. Sundberg, P. Fratzl, I. Burgert, Enhanced cellulose orientation analysis in complex model plant tissues, *J. Struct. Biol.* 183 (2013) 419, <https://doi.org/10.1016/j.jsb.2013.07.001>.
- [62] M. Zizek, C. Czibula, U. Hirn, The effect of the strain rate on the longitudinal modulus of cellulosic fibres, *J. Mater. Sci.* 57 (2022) 17517, <https://doi.org/10.1007/s10853-022-07722-7>.
- [63] C. Czibula, M.G. Simoes, M.H. Ulz, B.B. Ravanella, K. Elsayad, U. Hirn, K.J. Koski, The potential of Brillouin Spectroscopy for investigating the mechanical properties of hydrogels during dehydration, doi:10.48550/arXiv.2410.10883, 2024.
- [64] J. Andersson, E. Pori, E. Spärnäs, The effect of mechanical defects on the strength distribution of elementary flax fibres, *Compos. Sci. Technol.* 69 (2009) 2152, <https://doi.org/10.1016/j.compscitech.2009.05.010>.
- [65] A. Dal Fovo, J. Striova, D. Quintero Balbas, S. Mattana, N. Tacconi, R. Cicchi, R. Fontana, Nonlinear imaging and vibrational spectroscopic analysis of cellulosic fibres treated with COEX® flame-retardant for tapestry preservation, *RSC Adv.* 12 (2022) 26744, <https://doi.org/10.1039/d2ra02384a>.
- [66] L. Donaldson, Cellulose microfibril aggregates and their size variation with cell wall type, *Wood Sci. Technol.* 41 (2007) 443, <https://doi.org/10.1007/s00226-006-0121-6>.
- [67] C.J. Kennedy, G.J. Cameron, A. Šturmáková, D.C. Apperley, C. Altaner, T.J. Wess, M. C. Jarvis, Microfibril diameter in celery collenchyma cellulose: X-ray scattering and NMR evidence, *Cellulose* 14 (2007) 235, <https://doi.org/10.1007/s10570-007-9116-1>.
- [68] F. Barthelat, Z. Yin, M.J. Buehler, Structure and mechanics of interfaces in biological materials, *Nat. Rev. Mater.* 1 (2016) 16007, <https://doi.org/10.1038/natrevmats.2016.7>.
- [69] Y. Nishiyama, Structure and properties of the cellulose microfibril, *J. Wood Sci.* 55 (2009) 241, <https://doi.org/10.1007/s10086-009-1029-1>.
- [70] T. Maloney, J. Phiri, A. Zitting, A. Paajanen, P. Penttilä, S. Ceccherini, Deaggregation of cellulose macrofibrils and its effect on bound water, *Carbohydr. Polym.* 319 (2023) 121166, <https://doi.org/10.1016/j.carbpol.2023.121166>.
- [71] P.A. Penttilä, M. Altgen, M. Awais, M. Österberg, L. Rautkari, R. Schweins, Bundling of cellulose microfibrils in native and polyethylene glycol-containing wood cell walls revealed by small-angle neutron scattering, *Sci. Rep.* 10 (2020), <https://doi.org/10.1038/s41598-020-77755-y>.
- [72] M.J. Roach, N.Y. Mokshina, A. Badhan, A.V. Snegireva, N. Hobson, M. C. Deyholos, T.A. Gorshkova, Development of cellulosic secondary walls in flax fibers requires beta-galactosidase, *Plant Physiol.* 156 (2011) 1351, <https://doi.org/10.1104/pp.111.172676>.
- [73] J.C. Thimm, D.J. Burritt, W.A. Ducker, L.D. Melton, Pectins influence microfibril aggregation in celery cell walls: an atomic force microscopy study, *J. Struct. Biol.* 168 (2009) 337, <https://doi.org/10.1016/j.jsb.2009.06.017>.
- [74] J.C. Thimm, D.J. Burritt, W.A. Ducker, L.D. Melton, Celery (*Apium graveolens* L.) parenchyma cell walls examined by atomic force microscopy: effect of dehydration on cellulose microfibrils, *Planta* 212 (2000) 25, <https://doi.org/10.1007/s004250000359>.
- [75] K. Abe, H. Yano, Comparison of the characteristics of cellulose microfibril aggregates isolated from fiber and parenchyma cells of Moso bamboo (*Phyllostachys pubescens*), *Cellulose* 17 (2010) 271, <https://doi.org/10.1007/s10570-009-9382-1>.
- [76] A.N. Fernandes, L.H. Thomas, C.M. Altaner, P. Callow, V.T. Forsyth, D. C. Apperley, C.J. Kennedy, M.C. Jarvis, Nanostructure of cellulose microfibrils in spruce wood, *Proc. Natl. Acad. Sci. USA*. 108 (2011) E1195, <https://doi.org/10.1073/pnas.1108942108>.
- [77] L.H. Thomas, V.T. Forsyth, A. Sturcova, C.J. Kennedy, R.P. May, C.M. Altaner, D. C. Apperley, T.J. Wess, M.C. Jarvis, Structure of cellulose microfibrils in primary cell walls from collenchyma, *Plant Physiol.* 161 (2013) 465, <https://doi.org/10.1104/pp.112.206359>.
- [78] G. Chinga-Carrasco, Cellulose fibres, nanofibrils and microfibrils: the morphological sequence of MFC components from a plant physiology and fibre technology point of view, *Nanoscale Res. Lett.* 6 (2011) 417, <https://doi.org/10.1186/1556-276x-6-417>.
- [79] M. Gericke, K. Schlüter, T. Liebert, T. Heinze, T. Budtova, Rheological properties of cellulose/ionic liquid solutions: from dilute to concentrated states, *Biomacromolecules* 10 (2009) 1188, <https://doi.org/10.1021/bm801430x>.
- [80] K.S. Lefroy, B.S. Murray, M.E. Ries, Rheological and NMR studies of cellulose dissolution in the ionic liquid BmimAc, *J. Phys. Chem. B* 125 (2021) 8205, <https://doi.org/10.1021/acs.jpcc.1c02848>.
- [81] E. Richely, L. Nuez, J. Pérez, C. Rivard, C. Baley, A. Bourmaud, S. Guessasma, J. Beaugrand, Influence of defects on the tensile behaviour of flax fibres: cellulose microfibrils evolution by synchrotron X-ray diffraction and finite element modelling, *Compos. C: Open Access* 9 (2022) 100300, <https://doi.org/10.1016/j.jcomc.2022.100300>.
- [82] M. Müller, C. Cizhak, G. Vogl, P. Fratzl, H. Schober, C. Riekel, Direct observation of microfibril arrangement in a single native cellulose fiber by microbeam small-angle X-ray scattering, *Macromolecules* 31 (1998) 3953, <https://doi.org/10.1021/ma980004c>.
- [83] M. Müller, C. Cizhak, M. Burghammer, C. Riekel, Combined X-ray microbeam small-angle scattering and fibre diffraction experiments on single native cellulose fibres, *J. Appl. Crystallogr.* 33 (2000) 817, <https://doi.org/10.1107/S0021889800099751>.
- [84] C. Wang, N. Wang, S. Liu, L.-P.i. Choo-Simth, H. Zhang, Z. Zhi, Investigation of microfibril angle of flax fibers using X-ray diffraction and scanning electron

- microscopy, *J. Nat. Fibers* 17 (2020) 1001, <https://doi.org/10.1080/15440478.2018.1546639>.
- [85] F. Golek, P. Mazur, Z. Ryszka, S. Zuber, AFM image artifacts, *Appl. Surf. Sci.* 304 (2014) 11, <https://doi.org/10.1016/j.apsusc.2014.01.149>.
- [86] J.S. Villarrubia, Morphological estimation of tip geometry for scanned probe microscopy, *Surf. Sci.* 321 (1994) 287, [https://doi.org/10.1016/0039-6028\(94\)90194-5](https://doi.org/10.1016/0039-6028(94)90194-5).
- [87] S. Bardage, L. Donaldson, C. Tokoh, G. Daniel, Ultrastructure of the cell wall of unbeaten Norway spruce pulp fibre surfaces, *Nord. Pulp Pap Res. J.* 19 (2004) 448, <https://doi.org/10.3183/npprj-2004-19-04-p448-452>.
- [88] J. Fahlén, L. Salmén, On the lamellar structure of the tracheid cell wall, *Plant Biol.* 4 (2002) 339, <https://doi.org/10.1055/s-2002-32341>.
- [89] E.L. Hult, P.T. Larsson, T. Iversen, Cellulose fibril aggregation - an inherent property of kraft pulps, *Polymer* 42 (2001) 3309, [https://doi.org/10.1016/S0032-3861\(00\)00774-6](https://doi.org/10.1016/S0032-3861(00)00774-6).
- [90] E.L. Hult, P.T. Larsson, T. Iversen, A CP/MAS C-NMR study of supermolecular changes in the cellulose and hemicellulose structure during kraft pulping, *Nord. Pulp Pap Res. J.* 16 (2001) 33, <https://doi.org/10.3183/npprj-2001-16-01-p033-039>.
- [91] I. Duchesne, E. Hult, U. Molin, G. Daniel, T. Iversen, H. Lennholm, The influence of hemicellulose on fibril aggregation of kraft pulp fibres as revealed by FE-SEM and CP/MAS C-NMR, *Cellulose* 8 (2001) 103, <https://doi.org/10.1023/A:1016645809958>.
- [92] E. Richely, A. Bourmaud, V. Placet, S. Guessasma, J. Beaugrand, A critical review of the ultrastructure, mechanics and modelling of flax fibres and their defects, *Prog. Mater. Sci.* 124 (2022), <https://doi.org/10.1016/j.pmatsci.2021.100851>.
- [93] C. Plomion, G.g. Leprovost, A. Stokes, Wood Formation in trees, *Plant Physiol.* 127 (2001) 1513, <https://doi.org/10.1104/pp.010816>.
- [94] A. Khodayari, U. Hirn, A.W. Van Vuure, D. Seveno, Inverse rule of mixtures at the nanoscale: prediction of elastic properties of cellulose nanofibrils, *Composites Part A* 138 (2020) 106046, <https://doi.org/10.1016/j.compositesa.2020.106046>.
- [95] A. Khodayari, W. Thielemans, U. Hirn, A.W. Van Vuure, D. Seveno, Cellulose-hemicellulose interactions - a nanoscale view, *Carbohydr. Polym.* 270 (2021) 118364, <https://doi.org/10.1016/j.carbpol.2021.118364>.
- [96] V. Placet, O. Cissé, M. Lamine Boubakar, Nonlinear tensile behaviour of elementary hemp fibres. Part I: Investigation of the possible origins using repeated progressive loading with in situ microscopic observations, *Composites Part A* 56 (2014) 319, <https://doi.org/10.1016/j.compositesa.2012.11.019>.
- [97] M. Mattarelli, M. Vassalli, S. Caponi, Relevant length scales in Brillouin imaging of biomaterials: the interplay between phonons propagation and light focalization, *ACS Photonics* 7 (2020) 2319, <https://doi.org/10.1021/acsp Photonics.0c00801>.
- [98] A. Khodayari, U. Hirn, S. Spirk, Y. Ogawa, D. Seveno, W. Thielemans, Advancing plant cell wall modelling: atomistic insights into cellulose, disordered cellulose, and hemicelluloses – a review, *Carbohydr. Polym.* 343 (2024) 122415, <https://doi.org/10.1016/j.carbpol.2024.122415>.
- [99] J.P. Wolfe, *Imaging Phonons: Acoustic Wave Propagation in Solids*, Cambridge University Press, Cambridge, 1998.
- [100] K. Hofstetter, C. Hellmich, J. Eberhardsteiner, Development and experimental validation of a continuum micromechanics model for the elasticity of wood, *Eur. J. Mech. Solid.* 24 (2005) 1030, <https://doi.org/10.1016/j.euromechsol.2005.05.006>.
- [101] W.J. Cousins, Young's modulus of hemicellulose as related to moisture content, *Wood Sci. Technol.* 12 (1978) 161, <https://doi.org/10.1007/BF00372862>.
- [102] W.J. Cousins, Elastic modulus of lignin as related to moisture content, *Wood Sci. Technol.* 10 (1976) 9, <https://doi.org/10.1007/BF00376380>.